Pyridyl-Imidazole Copper Compounds

Alma Araujo Martinez[a], Christopher P. Landee[b], Diane A. Dickie[c], Jan L. Wikaira[d], Fan Xiao[b] and Mark M. Turnbull[a],

[a] Carlson School of Chemistry and Biochemistry, Clark University, 950 Main Street, Worcester, MA 01610, USA. E-mail: mturnbull@clarku.edu

[b] Department of Physics, Clark University, 950 Main Street, Worcester, MA 01610, USA

[c] Department of Chemistry, University of Virginia, Charlottesville, VA 22904 USA

[d] Department of Physical and Chemical Sciences, University of Canterbury, Private Bag 4800, Christchurch, New Zealand

Abstract

Three 4-(2'-pyridyl)imidazole (4-pyim) complexes of copper(II) have been synthesized and studied structurally and magnetically. The structures of $[CuCl_2(4\text{-pyim})]$ (**1**), $[CuCl(4\text{-pyim})_2]_2Cl_2(H_2O)_{10}$ (**2**) and $[Cu(CuCl_4)(4\text{-pyim})_2]$ $[Cu(H_2O)(4\text{-pyim})_2](CuCl_4)(H_2O)_4$ (**3**) are reported. Single-crystal X-ray diffraction measurements show that **1** crystallizes in the monoclinic space group $P2_1/n$ with a four-coordinate Cu(II) ion forming dimers via semi-coordinate bonds to bridging chloride ions. The structure of **1** shows the copper and chloride ions disordered over two sites. Compound **2** crystallizes in the triclinic space group *P*-1 with five-coordinate Cu(II) ions in a highly distorted geometry between square pyramidal and trigonal bipyramidal. It has an extensive hydrogen bonding network created by ten lattice water molecules, chloride ions and nitrogen atoms in the ligands. Compound **3** crystallizes in the monoclinic space group *C*c with both four and five-coordinate Cu(II) ions present in the lattice; the five-coordinate Cu(II) ions display highly distorted geometries. All three compounds present hydrogen bonding and π-stacking interactions among the 4-pyim rings. Magnetic susceptibility data were collected on **1**. Magnetic susceptibility data of **1** show that it exhibits modest antiferromagnetic interactions which are best fit using a honeycomb model [(2J = -2.6(2) K), 2J' = -1.6(2) K, $H = -2J \sum s_i \cdot s_j$]. Disorder in the crystal structure decreases the

rate of growth of the correlation length at low temperature, lowering the temperature of the expected maximum in χ below the range of the data.

Introduction

Chelating nitrogenous heterocyclic ligands have been widely used in coordination chemistry for a variety of applications. These ligands commonly consist of two or more rings that can be 6-membered, such as pyridine [1] and pyrazine [2], or 5-membered, such as pyrrole [3], imidazole [4] and triazole [5]. Examples of these chelating ligands are shown in Figure 1.

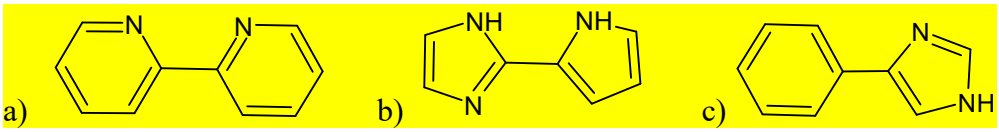

Figure 1. a) 2,2'-bipyridine b) 2,2'-biimidazole c) 4-(2'-pyridyl) imidazole

These ligands chelate to the transition metal ion through the nitrogen atoms, and the properties of the resulting compound are affected by the type(s) of ring involved. In these coordination compounds, the cationic metal ion coordinated to the nitrogen creates a combined effect that withdraws electron density from the rings, making them electron poor [6]. It is also known that while 6-membered rings are good π-acceptors, 5-membered rings are good π-donors [7]. In general, these nitrogen heterocycles have low π-electron density due to the electronegativity of the nitrogen atoms, which favors π-π stacking interactions in the packing of the molecules [6]. In addition, the size of the chelate rings favors the formation of complexes with metal ions of different sizes because of the steric strain [4]. Six-membered rings form short metal-nitrogen bonds favoring smaller metal ions, while 5-membered rings form longer metal-nitrogen bonds and favor larger metal ions [4].

Complexes of transition metal ions with 6-membered systems are the most common. There are more than ten thousand complexes of 2,2'-bipyridine (bipy), over seventeen hundred complexes of terpyridine and more than 50 complexes of 2,2'-bipyrazine with reported crystal structures [8]. There are significantly fewer reported structures of complexes with 5-membered

ring systems. There are more than 400 complexes of unsubstituted 2,2'-biimidazole (biim) and over 200 complexes with unsubstituted 2,2'-bipyrrole with reported crystal structures [8]. There are also complexes with mixed systems of 6- and 5-membered rings. There are over 150 complexes of unsubstituted 2-(2'-pyridyl)imidazole and 6 complexes of unsubstituted 2-(2'-pyridyl)-1H-pyrrole with reported crystal structures [8].

One of these mixed ring ligands is 4-(2'-pyridyl) imidazole, 4-pyim, shown in Figure 1c. There are fewer studies on the coordination chemistry of the 4-pyim ligand than on the related 5-membered and 6-membered related ligands, biim and bipy. There are 148 reported structures of transition metal complexes with the unsubstituted 4-pyim ligand, and of these only 31 contain copper [8]. Coordination compounds of 4-pyim have also been developed more recently in comparison to those of bipy and biim. The first compound with 4-pyim as a ligand, [Cu- (pyim)(l-1,5-dca)]NO_3 (dca = dicyanamide), was reported in 2002 [9]. Structures containing biim and bipy have been reported since the 1980s [8]. The 4-pyim contains three nitrogen atoms, two of which can chelate the metal ion, and the remaining nitrogen atom from the imidazole ring can be protonated or not according to the reaction conditions. The N-H group in the ligand can result in coordination complexes with hydrogen bonding throughout their lattice [10]. Some complexes with the 4-pyim ligand have been found to have weak antiferromagnetic (AFM) interactions, indicating the ligand is of interest in the study of magneto-structural correlations [9].

Copper(II) is considered an azaphilic species for its affinity to bond to nitrogen atoms, the reason that there are extensive studies of these types of compounds. This can be explained through the principle of hard and soft acids and bases (HSAB) developed by Pearson [11]. Copper(II) is classified as a borderline-hard Lewis acid, which favors the formation of compounds with borderline bases [12].While alkyl nitrogen species such as primary amines and ammonia are classified as hard bases, heterocyclic amines, such as pyridine, are borderline bases [11].

Here we report three new complexes with copper(II) and 4-pyim which were studied for their potential magnetostructural relevance. The syntheses, crystal structures and magnetic properties of [dichlorido-(4-(2'-pyridyl) imidazole)-copper(II)] (**1**) and bis[chlorobis(4-(2'-

pyridyl) imidazole) copper(II)] dichloride decahydrate dichloride (**2**) and the structure of [aqua-bis(4-(2'-pyridyl) imidazole) copper(II)][bis(4-(2'-pyridyl) imidazole) tetrachloridocuprate] tetrachloridocuprate(II) tetrahydrate (**3**) are presented.

Experimental

Materials and Methods

Copper(II) chloride dihydrate was purchased from Aldrich Chemical. 4-(2'-pyridyl) imidazole, 4-pyim, was purchased from Matrix Scientific. All chemicals were used as received. FTIR spectra were collected by ATR on a Perkin-Elmer Spectrum 100 IR spectrophotometer. X-Ray powder diffraction data were collected using a Bruker AXS-D8 Focus X-ray Powder Diffractometer. Elemental analyses were carried out by Marine Science Institute, University of California, Santa Barbara CA 93106.

Syntheses

[Dichlorido-(4-(2'-pyridyl)imidazole)-copper(II)] (**1**). 4-Pyim (0.178 g, 1.16 mmol) was dissolved in water (20 mL), giving a yellow turbid mixture, and the traces of insoluble material were removed through gravity filtration. HCl (0.75M, 1mL) was added dropwise to the solution until it reached pH 5. Copper chloride dihydrate (0.180 g, 1.05 mmol) was dissolved separately in water (10 mL), giving a turquoise solution. It was added to the 4-pyim solution, giving a dark green color. A saturated, aqueous, sodium chloride solution (1.835 g, 6 mL) was added to the mixture, and within ~10 minutes, small green crystals started forming. The reaction mixture was partially covered and left at room temperature for slow evaporation. The next day, dark green crystals were recovered through vacuum filtration, washed with water, and allowed to air dry. (Yield: 0.118 g **1**, 40% based on copper chloride dihydrate). CHN (%) Calculated(found): C: 34.36 (34.00), H: 2.52 (2.43), N: 15.03 (14.59). IR (m, cm^{-1}): 3185 m (broad), 1615 m, 1584 w, 1566 w, 1498 w, 1464 w, 1432 w, 1326 w, 1285 w, 1210 w, 1148 w, 1102 w, 1068 w, 1047 w, 1014 w, 978 w, 808 m, 764 m, 678 m, 643 w, 616 m.

Bis[chlorobis(4-(2'-pyridyl) imidazole) copper(II)] dichloride decahydrate dichloride (**2**). 4-Pyim (0.164 g, 1.07 mmol) was dissolved in water (15 mL), giving a yellow turbid mixture, and the traces of insoluble material were removed through gravity filtration. Copper chloride

dihydrate (0.097 g, 0.55 mmol) was dissolved separately in water (15 mL), giving a turquoise solution, and was added to the prior solution. HCl (5 drops, 1.5 M) was added to the reaction mixture, and the pH reached 3. A saturated, aqueous, sodium chloride solution (1.89 g, 5.5 mL) was added to the mixture, and a pale green powder was observed within a few minutes. This powder (0.129 g) was separated from the reaction mixture through gravity filtration, and it was determined to be amorphous through powder X-ray diffraction. IR (ν, cm^{-1}): 3345 m (broad), 3109 m, 2879 m, 1616 m, 1588 m, 1567 w, 1511 w, 1477 w, 1460 w, 1444 w, 1332 w, 1285 w, 1234 w, 1161 w, 1107 w, 1982 w, 1055 w, 1030 w, 971 w, 899 w, 818 w, 779 s, 684 m, 652 m, 622 m. The flask containing the filtrate of the reaction mixture was covered in parafilm and left at room temperature for slow evaporation. After ~1 week, irregular green crystals were recovered through vacuum filtration, and allowed to air dry. (Yield: 0.033 g green crystals of **2**, 11% based on imidazole-pyridine). No combustion analysis was attempted, due to the deliquescent nature of the compound. IR (ν, cm^{-1}): 3096 (m, very broad), 2946 w, 2881 w, 1616 w, 1587 w, 1510 w, 1477 w, 1443 w, 1330 w, 1283 w, 1236 w, 1161 w, 1107 w, 1081 w, 1053 w, 1029 w, 971 w, 774 s, 750, 685 m, 653 m, 623 m.

A few crystals of compound **3,** [aqua-bis(4-(2'-pyridyl) imidazole) copper(II)][bis(4-(2'-pyridyl) imidazole) tetrachloridocuprate(II)] tetrachloridocuprate(II) tetrahydrate, were produced serendipitously once during the preparation of **2** under the same reaction conditions. Multiple attempts to prepare **3** intentionally have been unsuccessful and thus only the structure is reported here.

X-Ray structure analysis

Data for **1** at 153 K and **3** at 168 K were collected on a CCD Area Detector diffractometer running Bruker SMART software [13] with Mo Kα radiation (λ = 0.71073 Å) with φ and ω scans employing a graphite monochromator. Cell parameters were refined using Bruker SMART [14] and absorption corrections were made using SADABS [15]. These crystal structures were solved using the SHELXS-14 program [16] and refined via least-squares analysis using SHELXL-2018 [17].

Data for **1** (at 100K and 303 K) and **2** were collected on a Bruker D8 Venture PhotonIII diffractometer running Bruker Instrument Service v6.2.15 software. An Incoatec IμS 3.0 micro-focus sealed X-ray tube (Mo Kα, λ = 0.71073 Å) with a HELIOS double bounce multilayer mirror monochromator were used for **1**, and an Incoatec IμS 3.0 micro-focus sealed X-ray tube (Cu Kα, λ = 1.54178 Å) with a HELIOS MX double bounce multilayer mirror monochromator were used for **2**. Cell parameters were refined using SAINT V8.40B [18], and absorption corrections were made with SADABS 2016/2 [19]. These structures were solved using the SHELXS-15 program [16] and refined via least-squares analysis using SHELXL-2018 [17].

Non-hydrogen atoms were refined anisotropically. Hydrogen atoms bonded to carbon atoms were placed in calculated positions and refined via a riding model using fixed isotropic thermal parameters. Hydrogen atoms bonded to oxygen or nitrogen were located in the difference Fourier maps and treated with fixed isotropic thermal parameters used during position refinement. Cell constants, refinement parameters, etc. are provided in Table 1. Selected bond lengths angles are given in Table 2 for compound **1** and Table **5** for compounds **2** and **3**.

Table 1. X-ray data collection and refinement parameters for **1-3**

	1, 100 K	**1,** 153 K	**1,** 303 K	**2**	**3**
Empirical formula	**$C_8H_7Cl_2CuN_3$**	**$C_8H_7Cl_2CuN_3$**	**$C_8H_7Cl_2CuN_3$**	**$C_{16}H_{24.50}Cl_2CuN_6O_{5.25}$**	**$C_{32}H_{34}Cl_8Cu_4N_{12}O_3$**
Formula weight (g/mol)	279.61	279.61	279.61	519.35	595.24
Temp (K)	100 (2)	153(2)	303(2)	100(2)	168 (2)
Wavelength (Å)	0.71073	0.71073	0.71073	1.54178	0.71073
Space group	Monoclinic, $P2_1/n$	Monoclinic, $P2_1/n$	Monoclinic, $P2_1/n$	Triclinic, P-1	Monoclinic, Cc
a (Å)	8.6023 (2)	8.694(3)	8.7052 (3)	12.5632(8)	21.891(7)
b (Å)	9.9108 (2)	9.973(4)	9.9517(3)	14.116(9)	14.750(4)
c (Å)	11.0919 (3)	11.186(4)	11.1710 (4)	14.1879(9)	13.946(5)
α (°)	90	90	90	71.535(3)	90
β (°)	97.7612 (11)	97.910(5)	96.7584 (12)	71.950(3)	99.433(6)
γ (°)	90	90	90	75.974(3)	90

Volume *(Å)*	936.98(4)	960.7(6)	961.04(6)	2239.2(3)	4442(2)
Z	4	4	4	2	4
Density (calc)	1.982	1.933	1.932	1.541	1.780
Abs. coef.	2.856	2.786	2.785	3.397	2.422
F(000)	556	556	556	1070	2384
Size (mm^3)	0.246x0.118x 0.048	0.3 x 0.29 x 0.20	0.152x0.141x 0.051	0.126 x 0.085 0.040	0.28 x 0.24 x 0.11
θ range (°)	2.767-30.513	2.748-27.732	2.812-30.519	3.345-68.433	2.128-27.669
Index ranges	$-12 \leq h \leq 12$	$-11 \leq h \leq 11$	$-10 \leq h \leq 12$	$-15 \leq h \leq 15$	$-28 \leq h \leq 28$
	$-13 \leq k \leq 14$	$-12 \leq k \leq 12$	$-10 \leq k \leq 14$	$-16 \leq k \leq 16$	$-18 \leq k \leq 9$
	$-15 \leq l \leq 15$	$-14 \leq l \leq 14$	$-15 \leq l \leq 12$	$-17 \leq l \leq 17$	$-18 \leq l \leq 17$
Reflections collected	2863	2139	2931	8185	9511
Independent reflections	2658	2033	2497	7110	8219
Abs.corr. type	Multi-scan	Multi-scan	Multi-scan	Multi-scan	Multi-scan
Max/min trans.	0.7461/0.6329	1.000/0.72147	0.7461/0.6220	0.637/0.858	1.0000/0.82845
Data / restraints / parameters	2863/0/158	2139/0/158	2931/0/158	8185/15/646	9511/14/578
Goodness-of-fit on F^2	1.085	1.239	1.044	1.031	0.933
Final *R* indices [$I>2\sigma(I)$]	0.0248	0.0275	0.0261	0.0465	0.0242
R indices (all data)	0.0276	0.0292	0.0341	0.0537	0.0320
Final diff. peak/hole	0.788/ -0.307	0.650/-0.313	0.435/-0.263	0.851/-0.495	0.624/-0.294

Magnetic Susceptibility Data Collection

Magnetization data of **1** were collected using a Quantum Design MPMS-XL SQUID magnetometer. Finely ground crystals were packed into a #3 gelatin capsule and placed in a clear plastic straw for data collection. Data were collected as a function of field from 0 to 50 kOe at 1.8 K. As the field was reduced to 0 kOe several data points were recollected to check for hysteresis effects; no hysteresis was observed. The M(H) response was linear beyond at least 5 kOe for all samples. Magnetization was also measured as a function of temperature from 1.8 to 310 K in a 1 kOe applied field. The data were corrected for the background signal (measured independently), the temperature independent paramagnetism of the Cu(II) ion and the diamagnetic contributions of the constituent atoms, estimated via Pascal's constants [20]. All data were fit using the Hamiltonian $H = -2J\Sigma S_1 \cdot S_2$. Powder X-ray diffraction data for **1** were compared to the single crystal structure prior to magnetic data collection to ensure that the sample was the same phase as the single crystal structure (See Supplementary Information, Figure SI-1). The deliquescent nature of **2** prevented powder X-ray and magnetic measurements.

Results and Discussion

Crystal Structure Analysis

Reaction of copper(II) chloride dihydrate with 4-pyim and sodium chloride in water gave **1**, which crystallized in the monoclinic space group $P2_1/n$ with 4 formula units in the unit cell. In the absence of the additional sodium chloride, crystallization is significantly slowed and side reactions (believed to result from air oxidation and hydrolysis of the ligand) become problematic. Selected bond lengths and angles are given in Table 2 and the local coordination sphere is shown in Figure 2. The copper ion is coordinated to two chloride ions and to one 4-pyim molecule through two nitrogen atoms. As shown in Figure 2, the copper ion and the two chloride ions are disordered over two sites, (Cu1, Cl1, Cl2 or Cu1a, Cl1a, Cl2a).

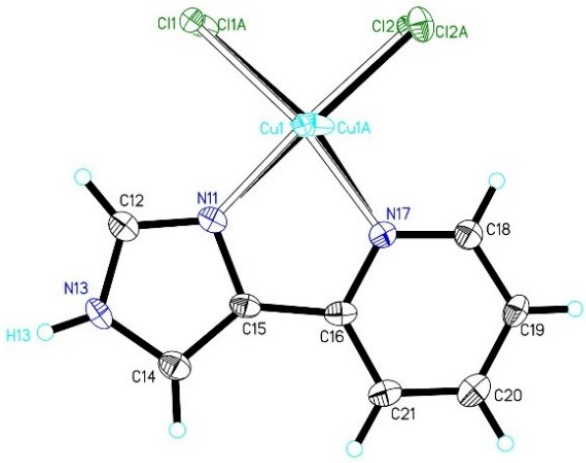

Figure 2. The molecular unit of **1** showing 50% probability thermal ellipsoids. Hydrogen atoms are shown as spheres of arbitrary size. Hollow bonds indicate the major component of the disordered ions (Cu1, Cl1, Cl2). Only hydrogen atoms whose positions were refined are labeled.

The crystal structure for **1** was obtained at three different temperatures (100 K, 153 K and 303 K), which had an effect in the occupancy factors of the disordered ions in addition to the unit cell dimensions. The different occupancy factors are displayed in Table 3. The occupancy changes from ~4:1 to ~2:1 as temperature increased by ~ 200 K. The disorder in this structure is unusual, because the heavier atoms are usually in fixed positions, while the light atoms from ligands or solvent molecules are disordered.

Table 2. Selected bond lengths (Å) and angles (°) for **1**. Angles are listed only for the major component.

	1 (100 K)	**1** (153K)	**1** (303 K)
Bond lengths (Å)			
Cu1-Cl1	2.267(4)	2.290(9)	2.275(5)
Cu1-Cl2	2.260(6)	2.28(1)	2.256(6)
Cu1-N11	1.954(3)	1.959(4)	1.948(3)
Cu1-N17	2.065(2)	2.077(4)	2.067(2)
Cu1A-Cl1A	2.264(16)	2.260(19)	2.239(12)
Cu1A-Cl2A	2.29(2)	2.29(2)	2.253(11)
Cu1A-N11	2.078(16)	2.090(14)	2.025(7)
Cu1A-N17	1.983(12)	2.023(9)	2.029(5)
Bond angles (°)			
Cl1-Cu1-Cl2	93.7(2)	93.3(3)	94.1(2)

N11-Cu1-N17	80.5(1)	80.7(1)	80.5(1)
Cl1-Cu1-N11	90.0(1)	90.2(3)	89.8(2)
Cl1-Cu1-N17	170.0(2)	170.5(3)	170.1(2)
Cl2-Cu1-N11	171.2(2)	171.4(3)	171.2(2)
Cl2-Cu1-N17	95.2(2)	95.3(3)	95.1(2)

Table 3. Occupancy factors of disordered ions for compound **1**

	100K	153 K	303 K
Cu1, Cl1, Cl2	0.81(2)	0.67(4)	0.66(3)
Cu1A, Cl1A, Cl2A	0.19(2)	0.33(4)	0.34(3)

In all the structures of **1**, each ring of the 4-pyim ligand is virtually planar within itself; the deviation of the constituent atoms from the mean plane of each is close to zero. The imidazole and pyridine rings are also virtually co-planar, with the angles between the mean planes of the imidazole and pyridine rings = 2.9°, 2.7° and 2.9° for the structures at 100 K, 153 K and 303 K respectively. For the major component of the disordered ions, the Cu(II) coordination sphere (Cu1, N11, N17, Cl1 and Cl2) is similarly planar with the mean deviations of the constituent atoms equal to 0.0450 Å, 0.0470 Å and 0.0491 Å for the structures at 100 K, 153 K and 303 K respectively. In all the structures, the two chloride ions are dislocated slightly to opposite faces of the Cu(II) coordination plane.

In the structures of **1**, the bite angles for the major component are 80.5(1)°, 80.7(1)° and 80.5(1)° while the bite angles for the minor components are 79.5(5)°, 79.0(4)° and 79.7(2)° at 100 K, 153 K and 303 K respectively. Structurally similar compounds to **1** have been reported to have bite angles ranging between 79° and 81°. $[Cu_2Cl_4L]$, where L is 1,4-bis[2-(2'-pyridyl)imidazol-1-yl]butane, has a bite angle of 79.89° [21], and $[CuL(Ph_3P)_2(Py\text{-}indz](BF_4)$, where Py-indz is 3-(pyridin-2-yl)imidazo[1,5-a]pyridine, has a bite angle of 79.49° [22]. Two similar compounds with the bipy ligand are $[Cu_2Cl_4(bipy)_2]$ with a bite angle of 81.0° [23] and $[CuBr_2(bipy)]_n$ with a bite angle of 80.0°[24]. A similar compound with the biim ligand is $[CuCl_2(Df\text{-}Me_2biim)]$ with a bite angle of 79.01°, where Df-Me_2biim is 2,2'-bi-1-Me-imidazole-5,5'-dicarboxaldehyde [25]. In these compounds, those with bipy ligands have

slightly larger bite angles than those with biim ligands. The compounds with mixed ligands of 6 and 5-membered rings have bite angles that fall in between those containing bipy or biim. Compound **1** packs as dimers [Cu···Cl distance of 2.895 Å], as shown in Figure 3.

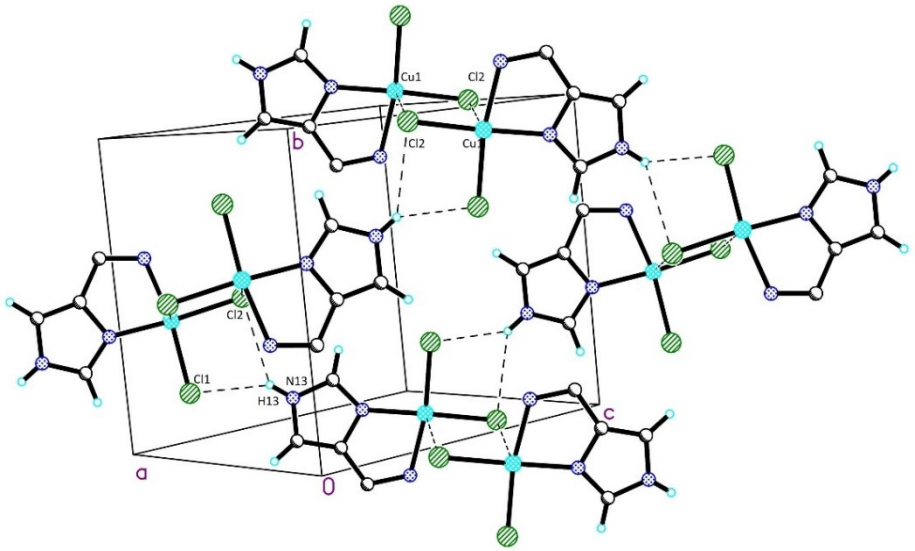

Figure 3. A packing diagram of **1** showing hydrogen bonding and dimer pairs via short Cu···Cl contacts (dashed lines). For clarity, only one set of the disordered ions is included in the figure.

Hydrogen bonding parameters for **1** are given in Table 4. Compound **1** presents bifurcated hydrogen bonding with N13 as donor and the chloride ions of the adjacent molecule as acceptors, as shown in Figure 3. The criteria for hydrogen bonding state that the bond angle D-H···A should be above 110° and the donor···acceptor distance should be less than the sum of the van der Waals (vdW) radii, although for weaker bonds the hydrogen-acceptor distance is a better indicator [26]. Bifurcated hydrogen bonds with two acceptors (A_1 and A_2) are known to have longer H···A distances and to be weaker than those in traditional hydrogen bonded structures [27]. These hydrogen bonds have been described in the literature through two additional criteria. Firstly, the sum of the angles associated with the hydrogen bond (D-H···A_1, D-H···A_2, A_1···H···A_2) is approximately 360°, and secondly, the hydrogen atom is within 0.2 Å of the plane composed of D, A_1 and A_2 [27]. All hydrogen parameters for **1** are within acceptable limits according to these criteria. As shown in Table 4, all H···Cl distances are below 2.95 Å, the sum of their vdW radii [28]. In addition, these parameters meet the criteria

for bifurcated hydrogen bonding. The sums of the angles N13-H13···Cl1, N13-H13···Cl2, and Cl1···H13···Cl2 for the structures of **1** at 100 K, 153 K and 303 K are 359.4°, 360.1° and 358.9°, respectively, while the distances of H13 to the plane formed by N13, Cl1 and Cl2, are 0.014 Å, 0.003 Å, and 0.032 Å, respectively.

Table 4. Hydrogen bonding parameters of **1** (100 K, 153 K, 303 K)

Structure/bond	D–H (Å)	H···A (Å)	D···A (Å)	D-H···A(°)
1 (100 K)				
N13-H13···Cl1	0.82(2)	2.45(3)	3.165(5)	145(2)
N13-H13···Cl2	0.82(2)	2.81(2)	3.462(5)	137(2)
1 (153 K)				
N13-H13···Cl1	0.87(3)	2.47(4)	3.22(1)	145(3)
N13-H13···Cl2	0.87(3)	2.80(3)	3.48(1)	136(3)
1 (303 K)				
N13-H13···Cl1	0.80(3)	2.51(3)	3.211(7)	146(2)
N13-H13···Cl2	0.80(3)	2.85(3)	3.490(6)	138(2)

Relevant trends in hydrogen bonding for comparison for **1** include hydrogen bonds with chloride acceptors and bifurcated hydrogen bonds in imidazole-containing structures. Chloride ions coordinated to transition metal ions are good acceptors for hydrogen bonding, and even in traditional hydrogen bonds, a significant number of these structures have long H···Cl distances [29]. A statistical study on the Cambridge Crystallographic Database (CSD) in the late 1990s showed that 42.6% of structures containing traditional hydrogen bonds of the form N-H···Cl-M have H···Cl distances between 2.52 Å and 2.95 Å [29]. Bifurcated hydrogen bonds have been reported to form in compounds containing protonated imidazole. In the imidazole-4-acetic acid/picric acid complex, a bifurcated bond forms between the N-H from the imidazole and oxygen atoms from nitro and phenol groups [30]. In the compound 5H-imidazo[4,5-f][1-10]phenanthroline, a bifurcated bond forms between the N-H from the imidazole ring and the nitrogen atoms of the phenanthroline ring of the adjacent molecules [31].

The dimer pairs connected through Cu···Cl short contacts are arranged into double-layers that can be observed when the packing of **1** is visualized parallel to the *b*-axis (Figure 4). These layers are stacked parallel to each other with no Cu···Cl contacts across layers. Within a layer

of dimers, the imidazole and pyridine rings of adjacent dimers are in close proximity to each other and there is evidence of π-stacking interactions amongst them. The N11-N17 centroid distance between adjacent dimer pairs within a layer are 3.657 Å, 3.693 Å and 3.734 Å for the structures at 100 K, 153 K and 303 K. Although there are no Cu···Cl contacts across the different layers, there is also evidence of π-stacking interactions between rings that are located in adjacent layers. The N11-N17 centroid distances between rings across different layers are 3.607 Å, 3.631 Å and 3.658 Å.

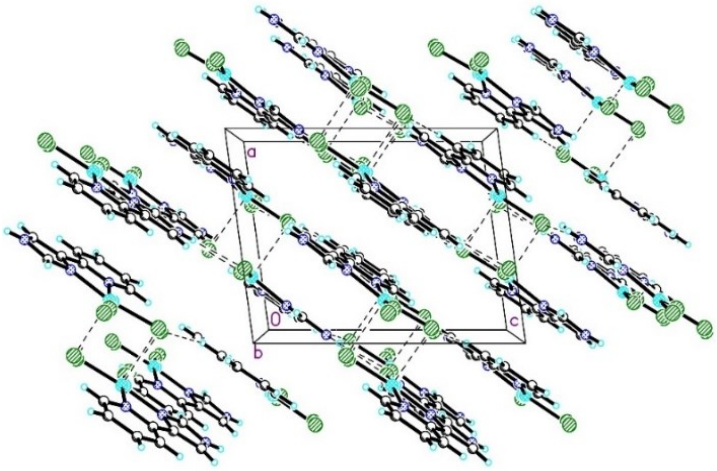

Figure 4. A packing diagram of **1** viewed parallel to the *b*-axis showing the packing of dimers. Dashed lines represent the Cu···Cl short contacts within the dimer pairs. For clarity, only one set of the disordered ions is included in the figure.

Structures with pyridine or imidazole rings that display π-stacking motifs can be found both in coordination complexes and purely organic molecules, and they are reported in the literature with similar centroid distances to those in **1**. For instance, the compound $[Cu(pyim)(tcm)_2]$, (where tcm is tricyanomethanide), has π-stacking between the pyridine rings of the ligand, with centroid distances that alternate between 3.9414 and 3.5986 Å [32]. The compound $[Cu(bipy)_2(H_2O)]\cdot[SiF_6]\cdot 4H_2O$ also has π-stacking amongst the pyridine rings, with centroid distances of 3.8774(12) Å [33]. The π-stacking motif is also present in nitrogen heterocyclic molecules not involved in coordination chemistry. The compound 5H-imidazo[4,5-f][1-10]phenanthroline displays π-stacking across imidazole and phenanthroline rings of its structure, with centroid distances of 3.631(8) Å [31].

Compound **2** crystallizes in the triclinic P-1 space group with 2 formula units in the unit cell and two crystallographically unique Cu(II) ions. Selected bond lengths and angles are given in Table 5 and the molecular unit is shown in Figure 5. Each copper ion is coordinated to two 4-pyim molecules and one chloride ion.

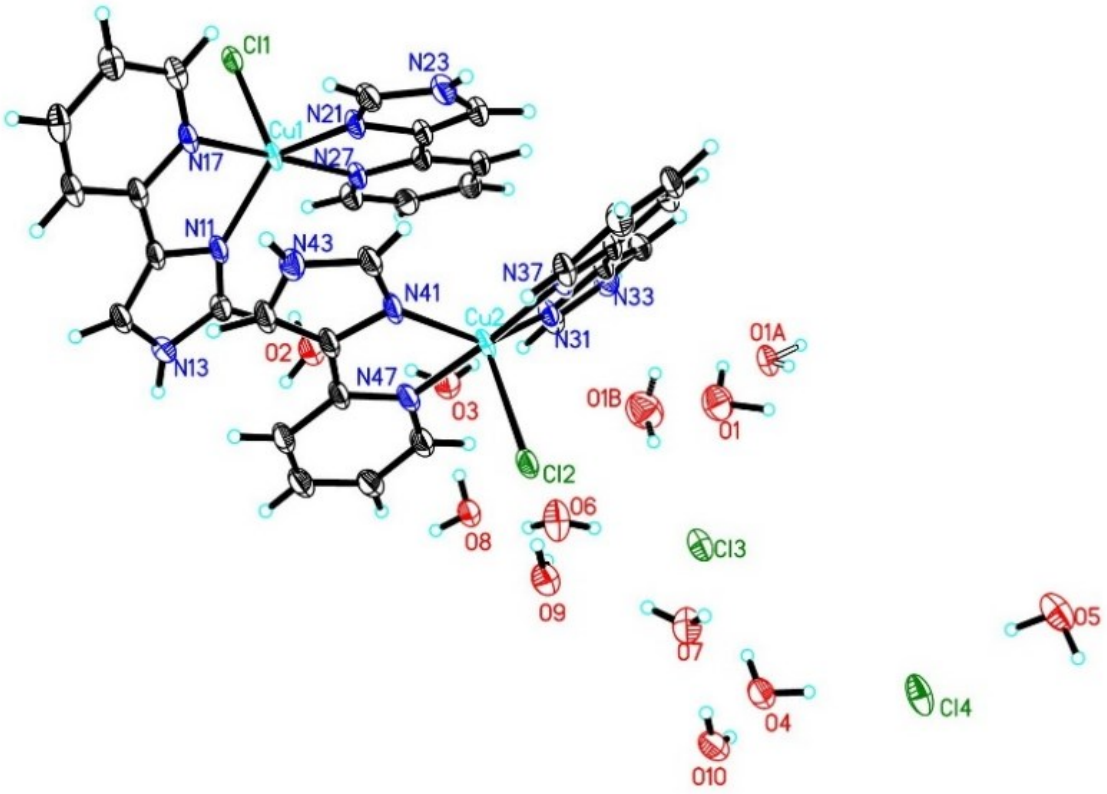

Figure 5. Thermal ellipsoid plot of the molecular unit of **2** showing 50% probability ellipsoids. Only the coordination sphere of Cu1 and Cu2 and the water molecules are labelled for clarity.

The individual coordination spheres of each copper ion are displayed in Figure 6, and it can be observed that both copper ions are five-coordinate. For atoms in the Cu1 ligands, adding 20 to the atom number results in the equivalent atom in the Cu2 ligands. The Addison parameters (τ) [34] for the individual Cu ions in compound **2** are Cu1 0.692 and Cu2 0.585, indicating that both have a highly distorted geometry that is in between square pyramidal and trigonal bipyramidal. Most of the bond lengths for the Cu coordination spheres are the same within

error. The Cu1-N11 bond, 2.041(2) Å, is longer than its equivalent Cu2-N31, 2.031(2) Å, and the Cu1-Cl1 bond 2.4261(8) Å, is shorter than its equivalent Cu2-Cl2, 2.4529(8) Å. In the case of the angles formed around the Cu ions, every angle is different within error, except for the corresponding bite angles.

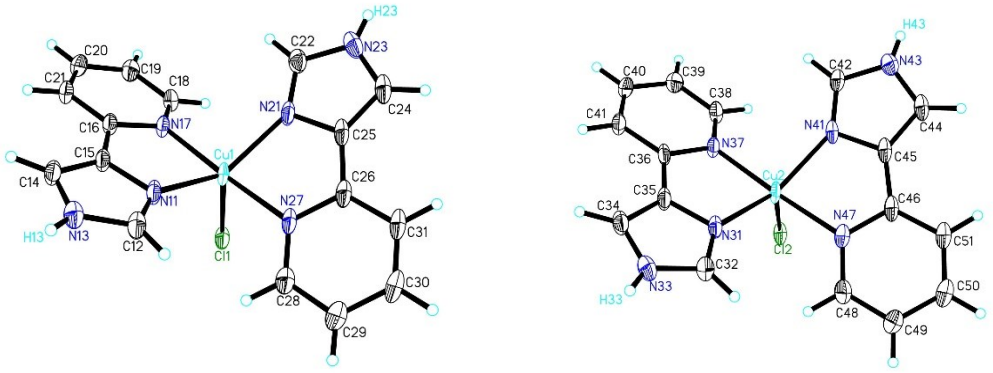

a) b)

Figure 6. Thermal ellipsoid plot of the coordination sphere of a) Cu1 and b) Cu2 in **2** showing 50% probability ellipsoids. Hydrogen atoms are shown as spheres of arbitrary size. Only hydrogen atoms that were refined are labeled.

In **2**, each 4-pyim ligand ring is virtually planar within itself; the deviation of the constituent atoms from the mean plane of each is less than 0.01 Å. The planes of the imidazole and pyridine rings of the same 4-pyim ligand have different degrees of planarity. In the Cu1 ion, the angles between the planes of the rings N11-N17 and N21-N27 are 2.7° are 4.8°, respectively. In the Cu2 ion, the angles between the planes of the rings N31-N37 and N41-N47 are 1.6° and 6.8° respectively. The five-membered rings formed by the copper ion, coordinated nitrogen atoms, and carbon atoms that bridge the 4-pyim ligand are also relatively planar. The angles formed between the mean planes of these rings within the same copper coordination sphere indicate that the different 4-pyim ligands are twisted. In the ligands of Cu1, the mean planes of N11 through N17 and of N21 through N27 are 0.0098 Å and 0.0154 Å, respectively, and they are at a 45.2° angle. In the ligands of Cu2, the mean planes of N31 through N37 and N41 through N47 are 0.0185 Å and 0.0305 Å, and they are at a 38.7° angle.

Table 5. Selected bond lengths (Å) and angles (°) for **2** and **3**.

	2	**3**
Bond lengths		
Cu1-N11	2.041(2)	1.996(3)
Cu1-N17	2.004(3)	2.019(3)
Cu1-N21	2.037(2)	2.009(3)
Cu1-N27	2.010(3)	2.020(3)
Cu1-Cl1	2.4261(8)	2.583(1)
Cu2-N31	2.031(2)	2.004(3)
Cu2-N37	2.000(2)	2.019(3)
Cu2-N41	2.040(3)	2.021(4)
Cu2-N47	2.013(2)	2.016(3)
Cu2-Cl2	2.4529(8)	-
Cu2-O1	-	2.175(3)
Bond angles (°)		
N11-Cu1-N17	81.5(1)	82.0(1)
N11-Cu1-N21	135.3(1)	149.8(1)
N11-Cu1-N27	98.4(1)	98.5(1)
N17-Cu1-N21	96.4(1)	99.0(1)
N17-Cu1-N27	176.8(1)	177.1(1)
N21-Cu1-N27	81.4(1)	81.9(1)
Cl1-Cu1-N11	111.48(7)	108.51(9)
Cl1-Cu1-N17	90.93(7)	88.86(9)
Cl1-Cu1-N21	113.22(7)	101.70(9)
Cl1-Cu1-N27	92.06(7)	88.25(9)
N31-Cu2-N37	81.68(9)	81.9(1)
N31-Cu2-N41	141.1(1)	148.1(1)
N31-Cu2-N47	98.6(1)	97.3(1)
N37-Cu2-N41	96.0(1)	100.1(1)

N37-Cu2-N47	176.2(1)	176.6(1)
N41-Cu2-N47	81.3(1)	82.4(1)
Cl2-Cu2-N31	113.33(7)	-
Cl2-Cu2-N37	92.51(7)	-
Cl2-Cu2-N41	105.52(7)	-
Cl2-Cu2-N47	90.80(7)	-
N31-Cu2-O1	-	119.4(1)
N37-Cu2-O1	-	91.6(1)
N41-Cu2-O1	-	92.4(1)
N47-Cu2-O1	-	86.0(1)

As shown in Figure 5, each copper coordination sphere resembles a highly distorted octahedron with a missing ligand in the axial position, and these coordination voids face each other. This causes the rings of the 4-pyim ligands of the different Cu ions to be spatially close. Figure 7 displays a packing diagram for **2**, in which it can be observed that this arrangement also places the ligands of adjacent molecular units in close proximity. The shortest centroid distances between the 4-pyim rings within a molecular unit are higher than literature reports for π-stacking interactions; the centroid distances of rings N11-N47 and N27-N31 are 4.285 Å and 4.247 Å, respectively. However, centroid distances between ligands of adjacent molecular units indicate these interactions are present; the N21 and N27 centroids in adjacent molecular units are 3.573 Å apart, and the N31 and N37 centroids in adjacent molecular units are 3.587 Å apart.

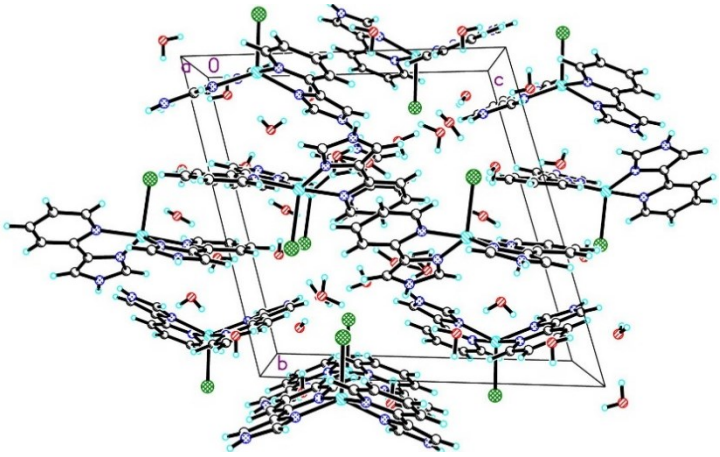

Figure 7. A packing diagram of **2** viewed parallel to the *a*-axis

In addition to the copper coordination spheres, **2** has two non-coordinated chloride ions and ten lattice water molecules. The large number of water molecules and chloride ions in addition to the protonated imidazole nitrogen in the 4-pyim ligands provides an extended network of hydrogen bonding. Hydrogen bonding parameters for **2** can be found in Table 6. The donor···acceptor distances and D-H···A angles describe the hydrogen bonding in **2**, given that these are traditional and not bifurcated. The protonated nitrogen atoms from the imidazole rings act as donors, of which only one of them, N33, hydrogen bonds to a chloride ion, while the others do so with oxygen atoms. The donor···acceptor distances range between 2.788(4) and 2.848(5) Å for N···O and 3.151(3) Å for N···Cl, which are all below the vdW radii sums of 3.07 Å and 3.27 Å respectively [28].

All the oxygen atoms from the water molecules in the lattice hydrogen bond to other oxygen atoms and chloride ions, both coordinated and those in the lattice. These hydrogen bonds with oxygen acceptors have O(donor)···O(acceptor) distances that range from 2.693(3) Å to 2.835(4) Å, which are all below the vdW radii sum of 3.04 Å [28]. The angles of all the bonds with oxygen atom acceptors range between 157(4)° and 175(4)°. The hydrogen bonds with chloride acceptors have O···Cl distances that range between 3.095(3) Å and 3.206(6) Å, which are all below the vdW radii sum of 3.27 Å [28]. The bond angles vary between 166(4)° and 177(4)°.

Table 6. Hydrogen bonding parameters for **2**

Bond	D–H (Å)	H···A (Å)	D···A (Å)	D-H···A(°)
Oxygen acceptor				
N23-H23···O1	0.79(4)	2.11(3)	2.848(5)	157(4)
O3-H3D···O2	0.77(5)	2.07(5)	2.829(4)	171(4)
O8-H8A···O3	0.80(3)	1.92(3)	2.718(3)	173(4)
N13-H13···O4	0.86(3)	1.94(3)	2.788(3)	172(4)
O10-H10B···O4	0.81(4)	1.97(4)	2.758(3)	165(4)
O3-H3E···O5	0.82(4)	1.96(4)	2.769(4)	172(4)
O9-H9A···O6	0.82(3)	1.88(3)	2.693(3)	175(4)
O10-H10A···O7	0.81(3)	1.91(3)	2.721(4)	173(4)
O1A-H1AA···O7	1.02(9)	1.80(9)	2.823(6)	177(8)
N43-H43···O8	0.78(4)	2.03(5)	2.792(4)	167(4)
O6-H6A···O8	0.80(4)	2.05(4)	2.805(3)	157(4)
O8-H8B···O9	0.79(3)	2.03(2)	2.802(3)	168(3)
O2-H2A···O10	0.83(2)	2.01(2)	2.835(4)	173(3)
O2-H2B···O10	0.82(2)	2.03(2)	2.829(3)	164(3)
Chloride acceptor				
O7-H7A···Cl1	0.87(4)	2.23(4)	3.129(2)	170(4)
O9-H9B···Cl2	0.88(5)	2.30(5)	3.177(2)	171(4)
O1-H1B···Cl3	1.0(1)	2.2(1)	3.206(6)	166(8)
O1A-H1AB···Cl3	0.82(5)	2.37(6)	3.171(4)	160(7)
O1B-H1BB···Cl3	0.85(4)	2.41(5)	3.195(7)	153(6)
O4-H4A···Cl3	0.81(5)	2.35(6)	3.145(3)	165(5)
O6-H6B···Cl3	0.82(5)	2.32(5)	3.136(3)	177(4)
O4-H4B···Cl4	0.95(5)	2.15(5)	3.095(3)	174(4)
O5-H5A···Cl4	0.94(6)	2.25(5)	3.170(3)	167(5)
O5-H5B···Cl4	0.97(5)	2.21(6)	3.155(3)	162(5)
N33-H33···Cl4	0.84(4)	2.33(4)	3.151(3)	166(4)

One of the water molecules is disordered over three sites, and it is represented with oxygen atoms O1, O1A and O1B. The formula of **2** indicates there are 10.5 water molecules per molecular unit, and the occupancies of each of these disordered molecules is 0.5. On one-half of the unit cells, only O1 is present, and in the remaining half, both O1A and O1B are present. When O1 is present neither O1A nor O1B can exist, because O1 is at 1.838(7) Å and 1.55(1) Å from O1A and O1B respectively. The distance between O1A and O1B is 3.167 Å, so their corresponding water molecules can be present at the same time.

Compound **3** crystallizes in the monoclinic *C*c space group with 4 formula units in the unit cell. Selected bond lengths and angles are given in Table 5, and the molecular unit is shown in Figure 8. It contains four crystallographically and structurally independent copper ions. Two of them, Cu1 and Cu2, are five-coordinate, and the other two, Cu3 and Cu4, are four-coordinate tetrachloridocuprate ions.

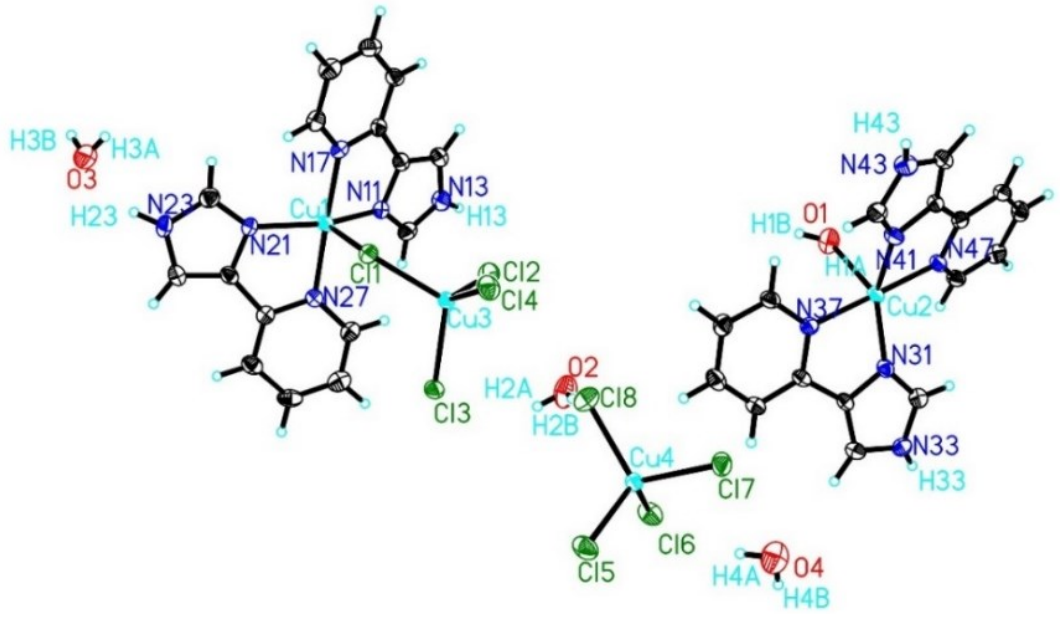

Figure 8. Thermal ellipsoid plot of the molecular unit of **3** showing 50% probability ellipsoids. Only the coordination sphere of the copper ions, water molecules, and hydrogen atoms involved in hydrogen bonding are labelled for clarity.

The individual coordination spheres of Cu1 and Cu2 are shown in Figures 9a and 9b respectively. For atoms in the Cu1 ligands, adding 20 to the atom number results in the equivalent atom in the Cu2 ligands. Cu1 and Cu2 are each coordinated to two 4-pyim molecules. In addition to the 4-pyim ligands, Cu1 is also coordinated to a tetrachloridocuprate ion (containing Cu3) through a bridging chloride ion, and Cu2 is also coordinated to a water molecule, making both Cu1 and Cu2 five-coordinate. The individual coordination spheres of Cu1 and Cu2 are displayed in Figure 10a and 10b respectively. In **3**, Cu1 has a τ value of 0.455, and Cu2 has a τ of 0.475, indicating that both have a distorted geometry that is in between the two idealized geometries for five-coordinate compounds.

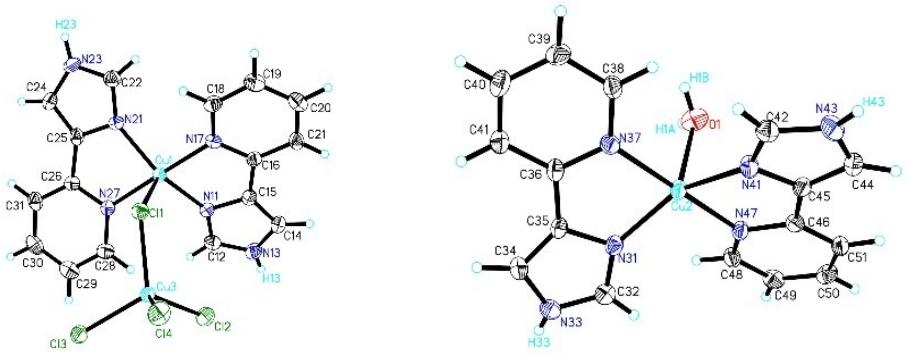

a) b)

Figure 9. Thermal ellipsoid plot of the coordination sphere of a) Cu1 and b) Cu2 in **3** showing 50% probability ellipsoids. Hydrogen atoms are shown as spheres of arbitrary size. Only hydrogen atoms that were refined are labeled.

In **3**, each ring of every 4-pyim ligand is virtually planar within itself; deviation from the mean plane of each one is less than 0.009 Å. The planes of the imidazole and pyridine rings of the same 4-pyim ligand are canted slightly to each other. In the ligands in the Cu1 ion, the angles between the planes of the rings N11-N17 and N21-N27 are 3.0° and 4.6° respectively. In the ligands in the Cu2 ion, the angles between the planes of the rings N31-N37 and N41-N47 are 4.3° and 4.5° respectively. As it happens in **2**, the different 4-pyim ligands within the same coordination sphere are twisted in **3**. In the ligands of Cu1, the mean planes of N11 through N17 and of N21 through N27 are 0.0163 Å and 0.0066 Å respectively, and they are at a 30.6° angle. In the ligands of Cu2, the mean planes of N31 through N37 and N41 through N47 are 0.0117 Å and 0.0267 Å, and they are at a 31.4°angle.

As shown in Figure 8, the coordination spheres of Cu1 and Cu2 in **3** are not facing each other within the same molecular unit as was observed in **2**. The presence of an additional $[CuCl_4]^-$ ion and the orientation and size of the axial ligands, $[CuCl_4]^{-2}$ and water, prevent this. However, in the packing of **3**, shown in Figure 10, it can be observed that the 4-pyim ligands from adjacent molecules are in close proximity of each other, leading to π-stacking interactions. The N41, N47 and N37 rings are close to N17, N11, and N21 of their adjacent molecular unit, respectively. The centroid distances of 3.609 Å for N41-N17, 3.884 Å for N41-N11, and 3.855 Å for N37-N21. The N17 ring is also close to the N47 ring of the adjacent molecular unit, with a centroid distance of 3.738 Å. Unlike **1** and **2**, **3** also has a π-stacking interaction between

pyridine rings only, as evidenced by the close distance of the N17 and N47 centroids. All the distances between centroids are in agreement with reported values for evidence of π-stacking interactions of structures containing imidazole and pyridine rings.

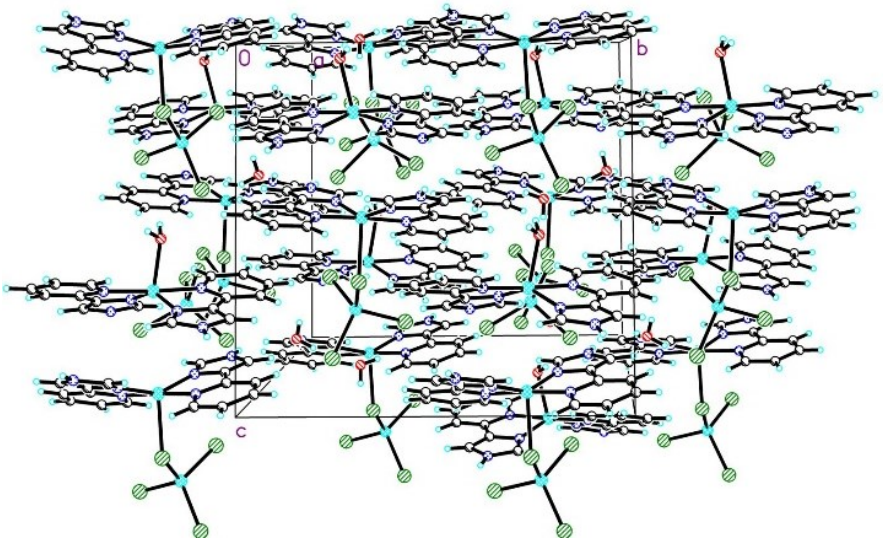

Figure 10. A packing diagram of **3** viewed parallel to the *c*-axis

The chloride ions in the tetrachloridocuprate ions, the water molecules and the protonated nitrogen atoms in the imidazole rings participate in hydrogen bonding in **3**. The hydrogen bonds with chloride ions as acceptors have H···Cl distances that range between 2.34(5) and 2.82(4) Å, which are all below the vdW radii sum of 2.95 Å [28]. Both Cl3 and Cl7 act as acceptors from two different donors; Cl1 and Cl8 do not participate in hydrogen bonding. The hydrogen bonds with oxygen atoms as acceptors have H···O distances that range between 1.89(4) and 2.16(4) Å, which are all below the vdW radii sum of 2.72 Å [28]. The bond angles vary from 125(4)° to 169(4)°.

Table 7. Hydrogen bonding parameters for **3**

Bond	D–H (Å)	H···A (Å)	D···A (Å)	D H···A(°)
Chloride acceptors				
N13-H13···Cl7	0.76(5)	2.53(5)	3.180(4)	146(5)
N33-H43···Cl3	0.72(4)	2.82(4)	3.285(4)	125(4)

N43-H43···Cl3	0.80(5)	2.46(5)	3.137(4)	144(4)
O1-H1B···Cl7	0.82(3)	2.34(4)	3.137(3)	164(4)
O3-H3B···Cl2	0.79(3)	2.50(3)	3.240(4)	157(4)
O4-H4B···Cl4	0.82(4)	2.35(4)	3.155(4)	169(4)
O4-H4A···Cl6	0.85(4)	2.39(4)	3.205(4)	159(4)
Oxygen acceptors				
N23-H23···O3	0.84(4)	2.05(4)	2.821(5)	151(4)
O1-H1A···O4	0.77(4)	1.89(4)	2.651(6)	167(4)
O3-H3A···O2	0.81(4)	2.16(4)	2.925(5)	157(4)

The bite angles of **2** range between 81.3(1)° and 81.68(9)°, and those of **3** range between 81.9(1)° and 82.4(1)°. A similar compound with the bipy ligand is $CuCl(bipy)_2]_2[Ge(HCit)_2]\cdot 8H_2O$ with bite angles of 79.94° and 79.72° [35].Two similar compounds with the biim ligand are $[Cu(biim)(C_2O_4)(H_2O)]H_2O$, with a bite angle of 82.55° [36] and $[Cu(biim)_2](ClO_4)\cdot$DMSO, with a bite angle of 82.22° [37]. In the case of these five-coordinate compounds with one or two nitrogen chelating ligands, those containing ligands five-membered rings have larger bite angles than those containing ligands with six-membered rings. Two compounds containing ligands with both six and five-membered rings have bite angles intermediate between those described above. Compound $[Cu(pyim)(mal)(H_2O)](H_2O)$, where mal is malonate, has a bite angle of 81.36° [38].Compound $[CuClL_2]$, where L is 3-pyridin-2-yl)imidazo[1,5-a]pyridine, has bite angles of 80.62° and 80.29° [39]. The bite angles of compounds **2** and **3** are comparable to those of structurally similar compounds reported in the literature.

Magnetic Data

Field dependent data at 1.8 K for **1** display downward curvature as shown in Figure 11, somewhat surprising for a low-dimensional magnetic system. Hysteresis was not observed, and M is linear from 0 to 20000 Oe. Compound **1** reached a maximum of 4540 emu mol^{-1} at 50 kOe. This value is below the expected saturation magnetization for Cu(II) compounds (~ 6,000 emu-mol^{-1}).

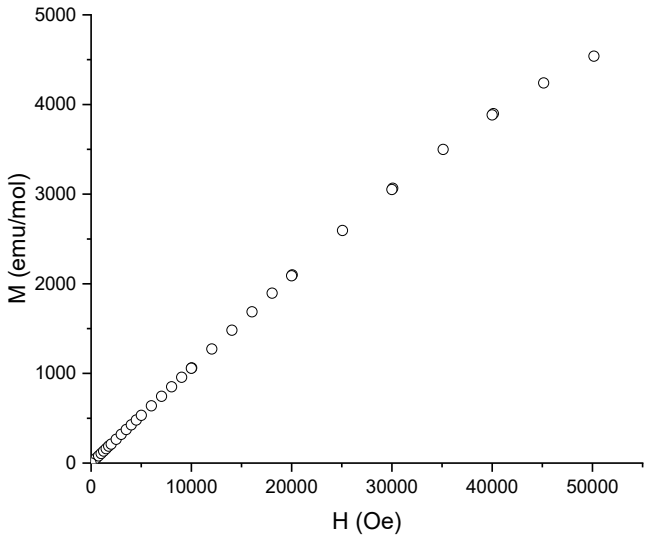

Figure 11. M(H) plot for **1**

The magnetic susceptibility as a function of temperature was measured from 1.8 K to 310 K in a 1 kOe field. χ(T) and 1/χ(T) are shown in Figure 122. χ(T) increases steadily as temperature decreases without any local maximum, as might be expressed in the presence of weak AFM interactions. The high temperature 1/χ(T) data were fit to the Curie-Weiss model (solid line in Figure 12), resulting in a Curie constant of 0.42 emu-K/mol-Oe and a Weiss constant of θ = -2.4 K. The small absolute value and negative sign of the Weiss constant is indicative of weak AFM interactions. The characteristic local maximum found in χ(T) plots of substances with AFM exchange could be absent in this case because it occurs at temperatures lower than 1.8 K or due to the disordered ions that create randomness in the crystal lattice (vide infra). The χT(T) graph in Figure 13, also shows evidence that **1** has modest AFM interactions, displaying downward curvature at low temperature, with a χT value that drops to 0.19 emu*K/Oe*mol at 1.8 K.

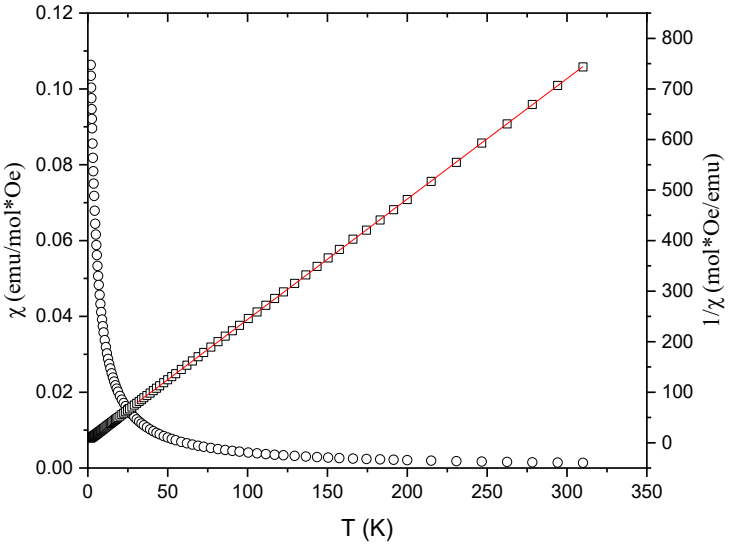

Figure 12. Magnetic susceptibility of **1** with χ(T) (open circles) and 1/χ(T) (open squares). The fit to the Curie-Weiss Law for 1/χ (T) is shown as a solid line.

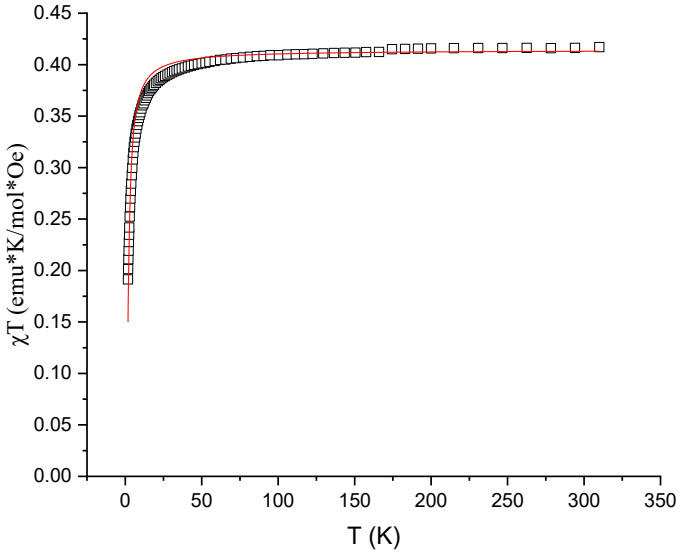

Figure 13. χT(T) plot of **1**. The fit to the dimer model is shown as a solid line.

Based on the dimer structure of **1**, the χ and χT data were fit to the AFM dimer model. Fitting parameters for these models are shown in Table 7.

Table 7. Summary table of the magnetic data fit parameters for **1**.

Dataset	CC	2J	Background	Reduced Chi-Sqr	R-Square (COD)
χ (first fit)	0.372(2)	-2.95(3)	-	1.40E-06	0.99845
χ (second fit)	0.42	-3.48(4)	-	8.36E-06	0.99065
χT	0.45(2)	-3.40(17)	-0.039(25)	7.39E-06	0.98997

The χ(T) data were fit to the AFM dimer model via two techniques, as shown in 4. The first fit, shown in a red solid line, was done without fixing any parameters, resulted in a Curie constant of 0.37 and 2J = -2.95 K. The second fit, shown in a dashed blue line, was done by fixing the Curie constant to the value obtained on the Curie-Weiss fit, 0.42 emu-K/mol-Oe and allowing the value of J to vary. This resulted in a slightly larger exchange constant of 2J = -3.48 K. Despite the difference in the magnetic exchange constant, both fits are of similar quality, as shown in their R-square values. The χT data were also fit to the dimer model (solid line in Figure 13). This fit is less accurate than the one for χ, as it can be observed in the graph and in its slightly lower R^2 value. The obtained 2J (-3.4 K) is within experimental error of the 2J obtained for the dimer fit of χ with a fixed Curie constant. There can be slight discrepancies in the parameters obtained from fitting the χ and the χT data because each one emphasizes different temperature regions. The fit of χ(T) gives more weight to the low temperature data, while the fit of χT(T) gives more weight to the high temperature data.

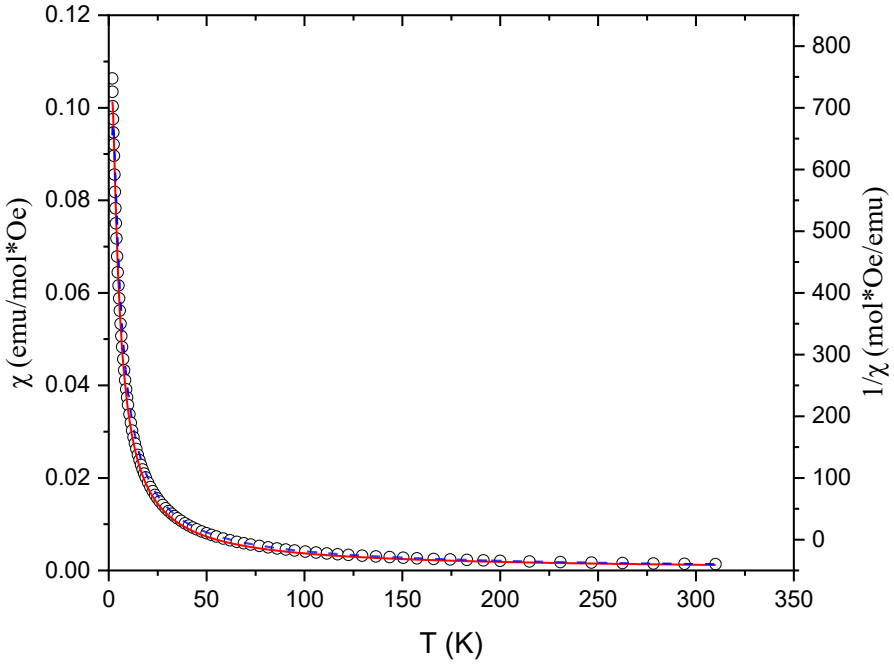

Figure 14. χT(T) plot of **1** fit to AFM dimer model. The solid red line is the fit allowing both J and C to vary; the dashed blue line is the fit with a fixed value of C, only allowing J to vary.

The small exchange constants obtained provide evidence that the maximum in the χ(T) plot may occur at lower temperatures. It is known that for a dimer with AFM interactions, this maximum occurs at the temperature of

$$T = 0.624\ J/k_B.[40]$$

The temperatures obtained with this formula are 1.8 K and 2.17 K for the J values of -2.951 K and -3.482 K respectively. The maximum may have not be detected because these temperatures are close enough to the lower limit reached by the instrument.

Quantum Monte Carlo simulations were performed to help in understanding the magnetic behavior of the compound employing the ALPS software [41]. Given the structure of the material (chloride bridged dimers) initial simulations were run using the Bleaney-Bowers equation [42] and fit the data well from RT down to ~ 7 K (with C = 0.395 emu-K/mol-Oe, 2J = -3.1(7) K) whereupon first an overestimation and then the appearance of a maximum in χ at lower temperature deviated significantly from the experimentally observed data (Figure 15).

In addition, the fitted Curie constant was significantly lower than that observed in the Curie-Weiss plot. Incorporation of a paramagnetic impurity provided a reasonable fit to the data down to 2.5 K with C = 4.13(1) emu-K/mol-Oe, in good agreement with the Curie-Weiss result, and 2J = -2.6(2) K (Figure 15). However, it required a 45% paramagnetic impurity which was not realistic in light of the combustion analysis data and powder X-ray diffraction pattern which matched the predicted pattern very well (see Figure SI-1).

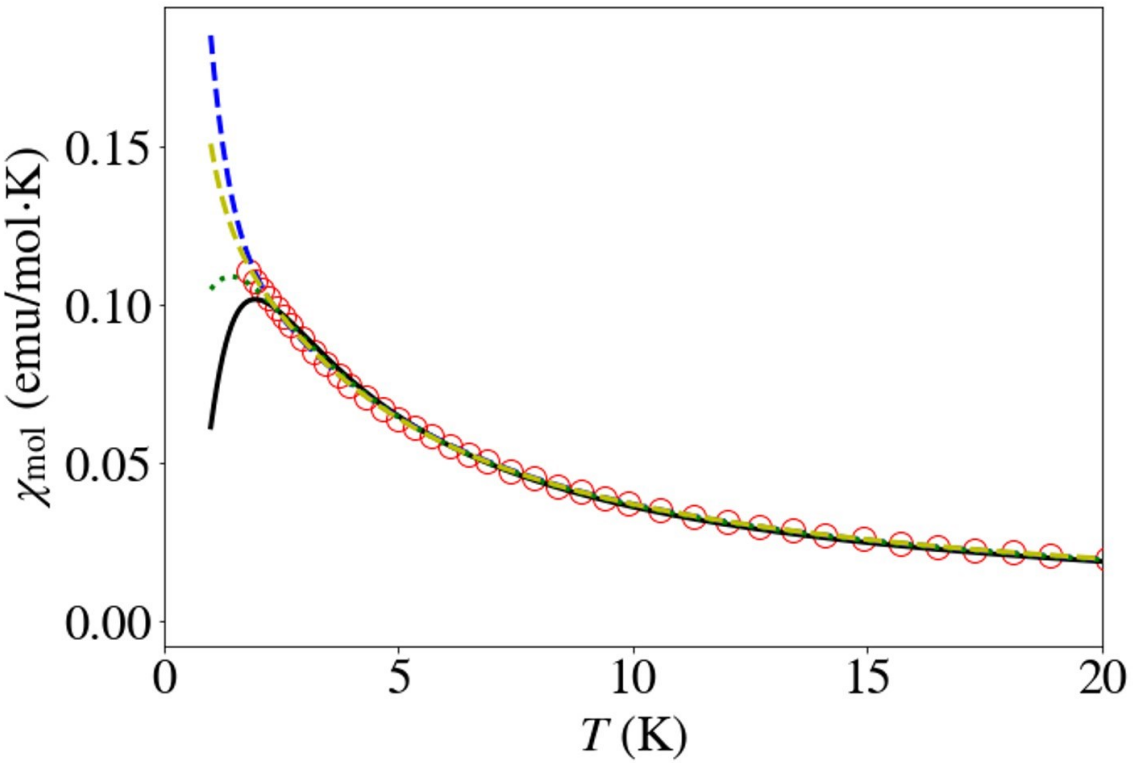

Figure 15. Simulation results using models for a simple dimer (solid black) or honeycomb (dotted green) model with no impurity. The open circles are the data. Introduction of a paramagnetic impurity into the dimer (dashed blue) or honeycomb (dashed yellow) model improved fit, but with unrealistic impurity % (see text for details). All fits are superimposable above 15 K.

The secondary superexchange pathway (via hydrogen bonding between dimers), with each chloride-bridged dimer acting as a double-donor, suggested the possibility of an alternating chain lattice which was also simulated, resulting in C = 0.413(3) emu-K/mol-Oe, 2J = -2.23(6) K and 2J' = -2.23(6) K (Figure 15). This would actually indicate a uniform chain, unlikely given the structure, and would be expected to show the onset of a maximum in χ at the lowest

temperatures, which was not observed. Incorporation of a paramagnetic impurity into the model provided an excellent fit over the entire temperature range, but required a 24% impurity – again unlikely given the purity of the sample as shown by combustion analysis and powder X-ray diffraction.

Consideration of each dimer unit as both a double hydrogen bond donor and a double hydrogen bond acceptor would generate a honeycomb arrangement of dimers (Figure 16). Simulation of a honeycomb lattice with two exchange constants (J within dimers and J' between dimers) via the ALPS software [41] produced the best match to the data down to 4 K with C = 0.414(3) emu-K/mol-Oe, 2J = -2.47 K and 2J' = -1.48 K (see Figure 17) if no paramagnetic impurity is incorporated in the model.

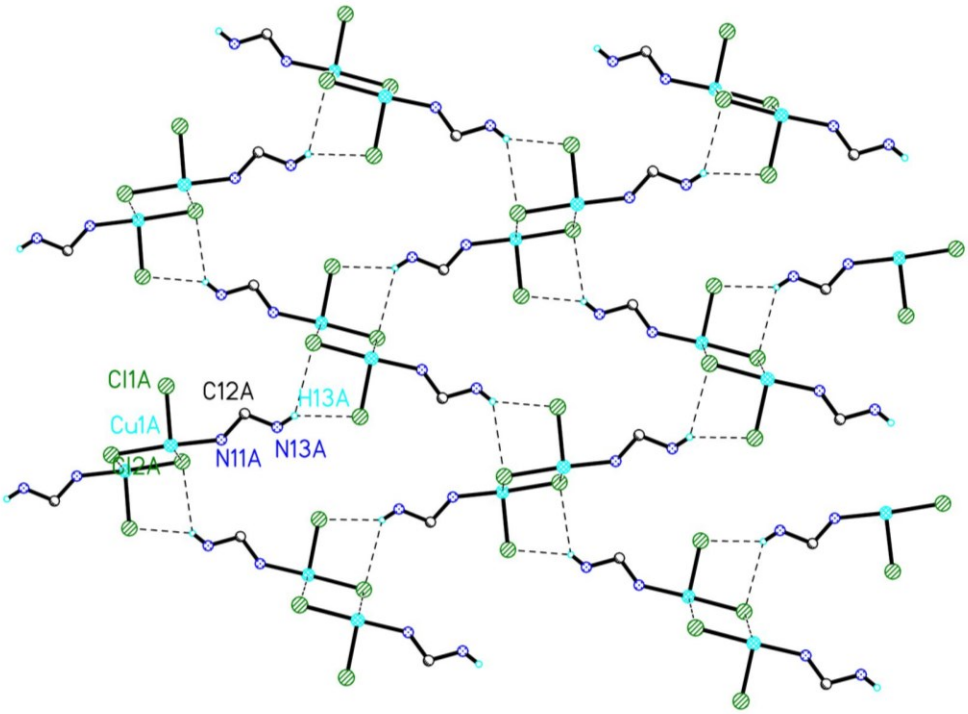

Figure 16. One layer of the structure of **1** showing the honeycomb lattice of dimers produced via hydrogen bonding. Only those atoms involved in the proposed superexchange linkages are shown for clarity.

Incorporation of a paramagnetic impurity produced a better overall fit over the entire temperature range with parameters C = 0.413(3) emu-K/mol-Oe, 2J = -2.6(1) K and 2J' = -

1.6(2) K and an 8.5 % paramagnetic impurity (see Figure 17). Although the fit was of good quality over the entire temperature range, it still seemed unlikely that an 8.5% paramagnetic impurity could be present and not easily detected by combustion analysis or powder X-ray diffraction.

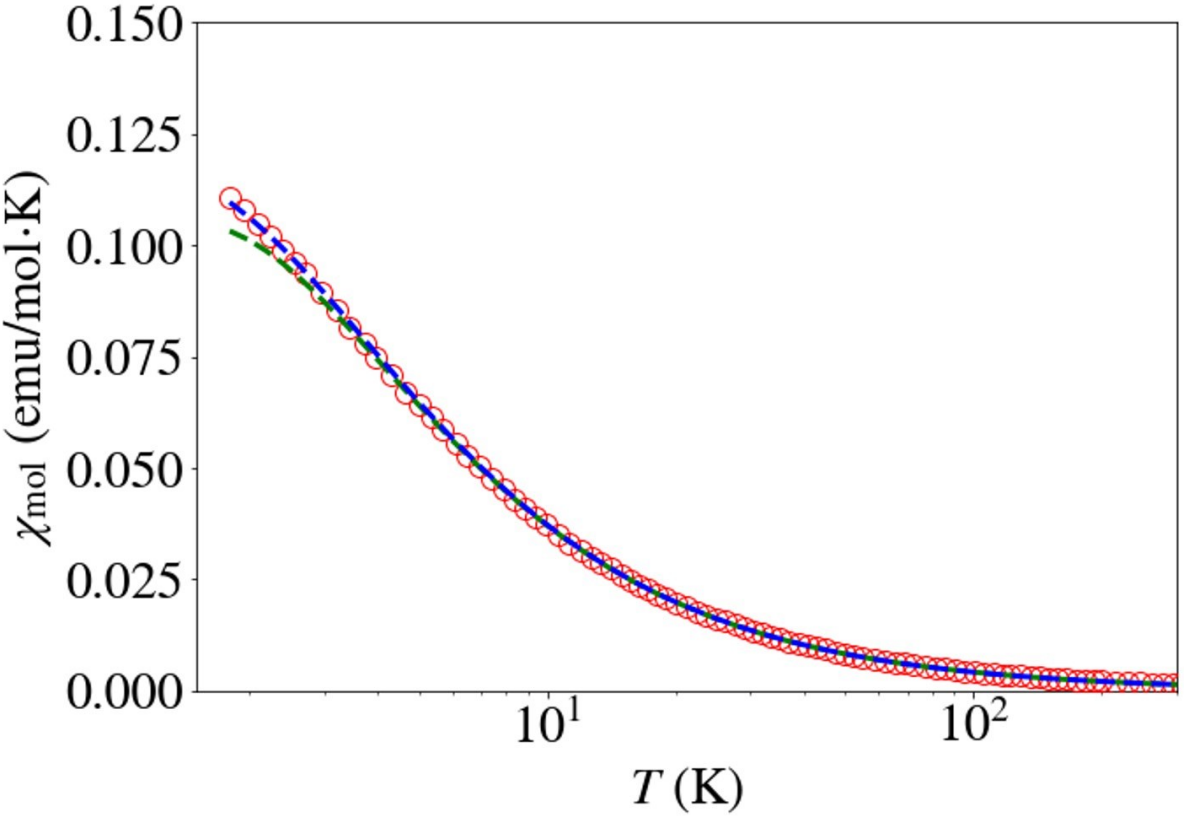

Figure 16 - ALPS simulations using a honeycomb model (2J = -2.47 K, 2J' = -1.48 K, dashed green line) or incorporating a paramagnetic impurity (8.5%, 2J = -2.6 K, J' = -1.6 K, dashed blue line). Open circles are the data. Note the log scale of the x-axis.

Although one would expect to see a maximum in χ for a dimer based upon any of these fitted values, none of the models incorporate the randomness factor introduced by the disorder in the complex. The disorder requires multiple exchange values within the chloride-bridged dimer units with Cu···Cl distances of 2.79(2) Å, 2.81(2) Å or 2.90(2) Å producing different values of J. Correlation lengths increase with decreasing temperature, assuming that the exchange is uniform. Introduction of randomness in the exchange will depress the rate of growth of the correlation length [43], lowering the temperature of the expected maximum, in this case below

1.8 K. Although qualitative, this explanation seems much more reasonable than the large impurity percentages that are required to fit the data with any of the existing models. Attempts to model the randomness would require data that incorporate the maximum in χ which must occur at a temperature below the range of our instrument.

Discussion

The magnetic properties of **1** can be explained through the Cu···Cl bridges formed within the dimer. Complexes of the form $[CuA_2X_2]$ and $[CuLX_2]$, where A is a monodentate ligand and L is a chelating ligand, can form dimers through Cu...Cl contacts with the chloride ion in the axial position of the metal, as shown in Figure 15 [44]. There are numerous complexes of this type that display cooperative magnetism, and the strength of the interactions has been correlated to geometric parameters of the dimer, which are the Φ angle, defined as the Cu-Cl-Cu' angle from the bridge, and R, defined as the longer Cu...Cl(axial) distance [44]. For the Φ/R ratio with values below 32.6°/Å and above 35.8°/Å, the compounds display AFM interactions, while compounds within this range display FM interactions [45]. For instance, the compound $[Cu(2\text{-pic})_2Cl_2]$, (2-pic= 2-methylpyridine) has a Φ/R ratio of 29.91°/Å and a J constant of -10.36 K, and compound $[Cu(Et_3en)Cl_2]$ a Φ/R ratio of 34.75°/Å and a J constant of 0.14 K [45]. On the compounds that have a ratio below 32.6°/Å, the exchange constant J is expected to increase along with Φ/R, but there is no direct proportionality [45]. In **1** the Φ/R ratios are 32.69°/Å, 29.94°/Å and 31.37°/Å for the structures obtained at 100, 153 and 303 K. These values are near the limit of 32.6°, where the compounds are expected to change from AFM to FM interactions, but as it is evidenced in the analysis of the magnetic data of **1,** the compound clearly has weak AFM interactions. If it is considered that the values of this ratio are in agreement with the AFM behavior of the compound, according to this correlation the exchange should be stronger. However, the disordered ions in **1** are Cu, Cl1 and Cl2, which are involved in the magnetic exchange. This affects the Φ/R ratio across the lattice, meaning the interaction might not happen to the same extent in every dimer, blurring the maximum.

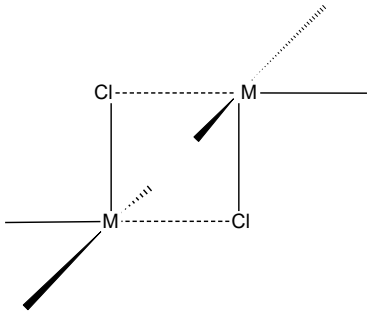

Figure 15. Tetragonal-pyramidal dimer arrangement

Conclusions

Two new copper(II) compounds with the ligand 4-pyim were studied for their magneto-structural correlations and a third one was studied structurally only. Their structures contain crystallographic disorder, hydrogen bonding to different extents and π-stacking interactions through the 4-pyim ligands.

Compound **1**, $[CuCl_2(4\text{-pyim})]$, was synthesized through slow evaporation. Single crystal X-ray showed that **1** contains four-coordinate copper(II) ions, and it displays an unusual crystallographic disorder, with copper and chloride ions disordered over two sites. The short Cu···Cl contacts of adjacent molecules creates dimers which are arranged into layers along the *b*-axis. The proximity of the rings from different 4-pyim ligands allows for π-stacking interactions. The compound also displays bifurcated hydrogen bonds from the protonated nitrogen atom of the imidazole ring towards the two chloride ions of the adjacent molecule. The magnetic susceptibility data show the complex has a weak AFM exchange. The data were modeled with an AFM dimer model and slightly different values were obtained for the Curie constant and magnetic exchange constant. The Curie constants obtained were 0.37(2), 0.42 and 0.45(2) for the χ, χT and $1/\chi$ fits respectively, while the 2J constants were -2.95(3), -3.48(4) and -3.40(17) for the χ, χ (with $1/\chi$ Curie constant) and χT fits respectively.

Compound **2**, $[CuCl(4\text{-pyim})_2]_2Cl_2(H_2O)_{10}$, was a hygroscopic product obtained serendipitously in the attempt to synthesize **3**, $[Cu(CuCl_4)(4\text{-pyim})_2][Cu(H_2O)(4\text{-pyim})_2][CuCl_4](H_2O)_3$. Single crystal X-ray showed that **2** displays two highly distorted five-coordinate copper(II) coordination centers with two 4-pyim ligands and one chloride ion in the

axial position. The geometry of the copper ions causes their coordination spheres to resemble a highly distorted octahedron with a missing ligand in the axial position, and the coordination voids of each one faces each other. As this motif extends throughout the lattice, rings from different 4-pyim ligands are in close proximity, causing π-stacking interactions. Compound **2** also has an extended hydrogen bonding network created by the lattice water, chloride ions and protonated nitrogen atoms from imidazole rings. All these hydrogen bonds are traditional, unlike those in **1.** One of the lattice water molecules is disordered over three sites. Preliminary magnetic data show the complex has little to no interactions, but due to the small sample mass and hygroscopic nature of the compound, further studies are needed to confirm the data.
Single crystal X-ray of compound **3** showed that it displays two highly distorted five-coordinate copper(II) coordination centers with two 4-pyim ligands and either a water molecule or a tetrachlorocuprate ion in the axial position. The close proximity of the 4-pyim ligands in adjacent molecules also creates π-stacking interactions in **3**. This compound also displays traditional hydrogen bonding to a lesser extent than **2**, and it does not contain disordered atoms.

Acknowledgements: The authors are grateful for funds from SEQENS toward the purchase of the D8 Focus diffractometer, from the National Science Foundation (IMR-0314773) for purchase of the MPMS SQUID magnetometer, and from the Kresge Foundation toward the purchase of both. In addition, we are grateful for funding from the NSF (CHE-2018870) toward the purchase of the PhotonIII diffractometer (U. Virginia). AAM is grateful for a summer fellowship from an anonymous donor.

Supplementary Information:
CCDC 2217089 (**1-100**), 2217090 (**1-153**), 2217093 (**1-303**), 2217091 (**2**) and 2217092 (**3**) contain the supplementary crystallographic data (CIFs). These data can be obtained free of charge via https://www.ccdc.cam.ac.uk/structures/, or from the Cambridge Crystallographic

Data Centre, 12 Union Road, Cambridge CB2 1EZ, UK; fax: (+44) 1223-336-033; or e-mail: deposit@ccdc.cam.ac.uk.

Figure SI-1 showing the comparison of the calculated and experimental powder patterns for compound **1**.

References

1. C. Kaes, A. Katz, M.W. Hosseini, *Chem. Rev.* **100**, 3553 (2000).
2. A) C. Bronner, O.S. Wenger, *Inorg. Chem*. **51**, 8275 (2012). B) R. Kirgan, M. Simpson, C. Moore, J. Day, L. Bui, C. Tanner, D.P. Rillema, *Inorg. Chem*. **46**, 6464 (2007). C). L. Marilena Toma, C. Eller, D.P. Rillema, C. Ruiz-Pérez, M. Julve, *Inorg. Chim*. *Acta*, **357**, 2609 (2004).
3. C.-M.Che, K.-K.Cheung, Z.-Y. Li, K.-Y. Wong, C.-C.Wang, Y. Wang, *Polyhedron*, **13**, 2563 (1994).
4. D. Buist, N.J. Williams, J.H. Reibsenspies, R.D. Hancock, *Inorg. Chem*. **49**, 5033 (2010)
5. J.G. Haasnoot, *Coord. Chem. Rev.* **200-202**, 131 (2000).
6. C. Janiak, *J. Chem. Soc., Dalton Trans.* 3885 (2000).
7. E.C. Constable, P.J. Steel, *Coord. Chem. Rev.* **93**, 205 (1989).
8. C. R. Groom, I. J. Bruno, M. P. Lightfoot, S. C. Ward, *Acta Cryst.* **B72**, 171 (2016). Version 5.43.
9. J. Carranza, J. Sletten, F. Lloret, M. Julve, *Polyhedron* **28**, 2249 (2009).
10. J. Martínez-Lillo, D. Armentano, G. De Munno, F. Lloret, M. Julve, J. Faus, *Dalton Trans.* 40 (2008).
11. R.G. Pearson, J. Songstad, *J. Am. Chem. Soc.*, **89**, 1827 (1967).
12. R. Griesser, H. Sigel, *Inorg. Chem.*, **9**, 1238 (1970).
13. SMART; cell refinement and data reduction, SAINT., Siemens analytical X-ray Instruments Inc.: Madison, WI, USA, 2000.
14. SMART: v.5.626, Bruker Molecular Analysis Research Tool, v.5.626; Bruker AXS: Madison, WI, USA 2002.
15. SADABS: v.2.01, an empirical absorption correction program, Bruker AXS Inc.: Madison, WI, USA 2001.
16. G.M. Sheldrick, *Acta Crystallogr., Sect. A:* **64**, 112 (2008)
17. G.M. Sheldrick, Ac*ta Crystallogr., Sect. C:*, **27** (2015).
18. SAINT V8.40B (Bruker Nano, Inc.), Madison, WI, USA 2019.
19. L. Krause, R. Herbst-Irmer, G.M. Sheldrick, D. Stalke, *J. Appl. Cryst.*. **48**, 3 (2015).
20. Carlin, R. L., *Magnetochemistry*. Springer-Verlag Berlin Heidelberg: Germany, 1986.
21. Y.-Q. Lan, Y.-M. Fu, K.-Z. Shao, Z.-M. Su, *Acta Crystallogr., Sect. E*:, **E62**, m2586 (2006).
22. C.M. Alvarez, L. Alvarez Miguel, R. García-Rodríguez, J. Martín-Alvarez, D. Miguel, *Eur. J. Inorg. Chem.* 4921 (2015).
23. G.E. Kostakis, E. Nordlander, M. Haukka, J.C. Plakatouras, *Acta Crystallogr., Sect. E:*, **62**, m77 (2006).
24. M.T. Garland, D. Grandjean, E. Spodine, A.M. Atria, J. Manzur, *Acta Crystallogr., Sect. C:*, **44**, 1209 (1988).
25. R. Tatikonda, E. Kalenius, M. Haukka, *Inorg. Chim. Acta*, **453**, 298 (2016).
26. E. Arunan, G. Desiraju, R. Klein, J. Sadlej, S. Scheiner, I. Alkorta, D. Clary, R. Crabtree, J. Duannenberg, P. Hobza, H. Kiaergaard, A. Legon, B. Mennucci, D. Nesbitt, *Pure Appl. Chem.*, **83**, 1637 (2010).

27. S.J. Grabowski, Chapter 1: Hydrogen Bond – Definitions, Criteria of Existence and Various Types. In *Understanding Hydrogen Bonds: Theoretical and Experimental Views*, The Royal Society of Chemistry: 2021; pp 1-40.
28. A. Bondi, *J. Phys. Chem*., **68**, 441 (1964).
29. G. Aullón, D. Bellamy, A. G. Orpen, L. Brammer, E.A. Bruton, *Chem. Commun.*, 653 (1998).
30. Y. In, H. Nagata, M. Doi, T. Ishida, A. Wakahara, *Acta Crystallogr., Sect. C*: **53**, 367 (1997).
31. S.-W. Tong, W.-D. Song, D.-L. Miao, J.-B.An, *Acta Crystallogr., Sect. E:* **68**, o1448 (2012).
32. C. Yuste, D. Armentano, N. Marino, L. Cañadillas-Delgado, F.S. Delgado, C. Ruiz-Pérez, D.P. Rillema, F. Lloret, M. Julve, *Dalton Trans.* 1583 (2008).
33. M. Nisbet, E. Hiralal, K. Poeppelmeier, *Acta Crystallogr., Sect. E:* **77,** 158 (2021).
34. A.W. Addison, T.N. Rao, J. Reedijk, J. van Rijn, G.C. Verschoor, *J. Chem. Soc., Dalton Trans.* 1349 (1984).
35. I. Seifullina, E. Martsinko, O. Chebanenko, O. Pirozhok, V. Dyakonenko, S. Shishkina, *Chem. J. Moldova*, **11**, 52 (2016).
36. J. Carranza, C. Brennan, J. Sletten, B. Vangdal, P. Rillema, F. Lloret, M. Julve, M., *New J. Chem.*, **27**, 1775 (2003).
37. Q.-H. Jin, L.-L. Zhou, L.-J. X u, Y.-Y. Zhang, C.-L. Zhang, X.-M. Lu, , *Polyhedron*, **29**, 317 (2010).
38. F.S. Delgado, F. Lahoz, F. Lloret, M. Julve, C. Ruiz-Pérez, *Cryst. Growth Des.*, **8**, 3219 (2008).
39. J.J.K. Carson, C.E. Miron, J. Luo, J.-L. Mergny, L. van Staalduinen, Z. Jia, A. Petitjean, *Inorg. Chim. Acta*, **518**, 120236 (2021).
40. C.P. Landee, M.M. Turnbull, *J. Coord. Chem.*, **67**, 375 (2014).
41. B. Bauer, L.D. Carr, H.G. Evertz, A. Feiguin, J. Freire, S. Fuchs, L. Gamper, J. Gukelberger, E. Gull, S. Guertler, A. Hehn, R. Igarashi, S.V. Isakov, D. Koop, P.N. Ma, P. Mates, H. Matsuo, O. Parcollet, G. Pawłowski, J.D. Picon, L. Pollet, E. Santos, V.W. Scarola, U. Schollwöck, C. Silva, B. Surer, S. Todo, S. Trebst, M. Troyer, M.L. Wall, P. Werner, S. Wessel (ALPS collaboration) *J. Stat. Mech*. P05001 (2011).
42. B. Bleaney, K.D. Bowers *Proc. R. Soc. London, A*, **214**, 451 (1952).
43. Zachar, O. *Phys. Rev. B* **62**, 13835 (2000).
44. W.E. Marsh, K.C. Patel, W.E. Hatfield, D.J. Hodgson, *Inorg. Chem.*, **22**, 511 (1983)
45. W.A. Alves, R.H. R. H. de Almeida Santos, A. Paduan-Filho, C.C. Becerra, A.C. Borin, A.M. da Costa Ferreira, *Inorg. Chim. Acta* **357**, 2269 (2004).